ELSEVIER

Ultramicroscopy 71 (1998) 21–29

ultramicroscopy

Near-field optical imaging using metal tips illuminated by higher-order Hermite–Gaussian beams

Lukas Novotny, Erik J. Sánchez, X. Sunney Xie

Pacific Northwest National Laboratory, Environmental Molecular Sciences Laboratory, P.O. Box 999, Richland, WA 99352, USA

Abstract

We propose a new scheme for high-resolution near-field optical imaging. The method relies on the highly enhanced fields at sharp metal tips under laser illumination. These fields are laterally confined to the tip size and can be used to locally excite the sample surface. Illumination along the tip axis with a higher-order beam mode (Hermite–Gaussian (1,0) mode) and detection of nonlinear responses (two-photon fluorescence, generation of second/third harmonics) ensure sufficient background discrimination. We outline the theory of laser beams beyond the paraxial approximation and investigate the electromagnetic fields for the proposed scheme.

Keywords: Near-field optics; Single molecule detection; Fluorescence imaging; Nonlinear optics; Nanotechnology

1. Introduction

Advances in near-field optics have brought the wealth of optical measurements to a dimension beyond the diffraction limit. Generally, a highly confined optical field between probe and sample is a prerequisite for high resolution in near-field optical microscopy. The resolution of commonly used aperture probes [1] is limited to ≈ 50 nm due to the low light throughput as well as the low reproducibility associated with the grain size of the aluminum coating. An apertureless configuration based on optical phase sensitive detection [2] has been put forward. While the resulting optical images have higher resolutions, they usually exhibit strong correlations with topography. For the resonant optical detection used (detection and illumination at the same wavelength), topographic features have intrinsically strong influence on the optical contrast. Background free imaging, such as fluorescence imaging, is less sensitive to this complication.

Fluorescence detection of single molecules with near-field microscopy attracted considerable attention, because it enables simultaneous *spectral* and sub-diffraction *spatial* measurements [3]. Furthermore, *temporal* resolved experiments allow studies of molecular dynamics on a nanometer scale. If molecules are sufficiently dispersed on a surface, a more sensitive detection has been obtained with tightly focused laser beams [4,5] using high numerical aperture objective lenses. However, for various other applications, such as imaging of single proteins in photosynthetic membranes [6], it is desirable to extend the resolution of fluorescence imaging to the 10 nm range.

0304-3991/98/$19.00
PII S0304-3991(97)00077-6

In this paper, we present a new scheme for high-resolution optical imaging. The method combines both far-field and near-field techniques and relies on the field enhancement at a metal tip. This field enhancement can be established by appropriate laser illumination. It has been proposed to use this effect for different near-field optical applications [7–14].

If the incident radiation has a polarization component along the tip axis, a strong surface charge density is induced at the tip end, giving rise to the field enhancement effect [7]. However, illumination along the tip axis with an ordinary laser beam (fundamental Gaussian mode) does not provide any polarization component along the tip axis and thus does not lead to a field enhancement at the tip end. While the desired polarization can be obtained by illuminating the tip from the sides, it is difficult to confine at the same time the exposure of the sample to the incident radiation. Oblique incidence increases the illuminated sample area leading to a higher background signal and faster sample damage. In the proposed scheme (Fig. 1), a metallic tip is located in the highly focused region of an on-axis laser beam of higher order (Hermite–Gaussian (1,0) mode). As will be shown in the theoretical analysis, this mode provides a longitudinal electric field in the focal region and therefore enables the field enhancement. The highly confined fields close to the tip locally interact with the sample surface. The sample's optical response, such as molecular fluorescence, is collected by the same high N.A. objective lens as used for illumination. In order to discriminate the background signal from the entire illuminated region against the signal from the region of enhanced field, it is advantageous to detect nonlinear optical responses of the sample (two-photon fluorescence, generation of second/third harmonics, etc.) because the nonlinear signals are proportional to higher powers of the field intensity.

It has been proposed to use the longitudinal field of the Hermite–Gaussian (1,0) mode to accelerate charged particles along the beam axis in linear particle accelerators [15]. Recently, Trautman and Macklin used the longitudinal field in a far-field microscope to image the spatial orientation of molecular transition dipoles [16]. The theoretical analysis described below will not only be useful for the proposed near-field experiment, but also instructive to various far-field applications.

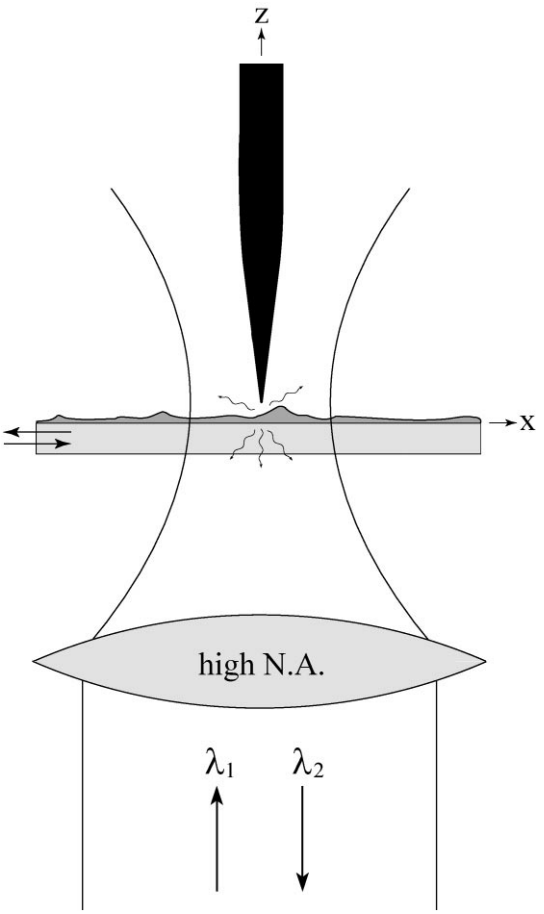

Fig. 1. Configuration of the proposed scheme. A highly focused Hermite–Gaussian (1,0) beam is used to illuminate a metal tip in axial direction (λ_1). The longitudinal fields at the focus give rise to a strong field enhancement at the tip. The tip field interacts locally with the sample surface. Nonlinear optical responses (two-photon fluorescence, generation of second/third harmonics) are detected in order to suppress the background signal (λ_2).

2. Theory

2.1. Fields in the focal region of a laser beam

In many textbooks, laser beams are described by the first order, paraxial approximation leading to

purely transverse fields [17]. This approximation is not valid in the focal region of a highly focused beam for which higher-perturbation orders need to be considered. This section is intended to give an accurate description of laser modes and to investigate the longitudinal field components of the fundamental Gaussian mode (Hermite–Gaussian (0,0) mode) and the Hermite–Gaussian (1,0) mode.

A time-harmonic laser beam in a homogeneous medium must fulfill Maxwell's curl equations

$$\nabla \times \boldsymbol{E}(\boldsymbol{r}) = \mathrm{i}k[Z_{\mu\varepsilon}\,\boldsymbol{H}(\boldsymbol{r})], \tag{1}$$

$$\nabla \times [Z_{\mu\varepsilon}\,\boldsymbol{H}(\boldsymbol{r})] = -\mathrm{i}k\boldsymbol{E}(\boldsymbol{r}), \tag{2}$$

where $Z_{\mu\varepsilon} = [\mu_0\mu/\varepsilon_0\varepsilon]^{1/2}$ is the wave impedance of the medium. Any solution to Eq. (1) and (2) can be represented by two scalar fields that satisfy the scalar Helmholtz equation and fulfill the appropriate boundary conditions [18]. Following the approach of Barton and Alexander [19] these scalar fields can be chosen as one component vector potentials

$$\boldsymbol{A}_{\mathrm{e}}(\boldsymbol{r}) = A(\boldsymbol{r})\boldsymbol{n}_x, \tag{3}$$

$$\boldsymbol{A}_{\mathrm{m}}(\boldsymbol{r}) = A(\boldsymbol{r})\boldsymbol{n}_y, \tag{4}$$

where $A(\boldsymbol{r})$ fulfills the Helmholtz equation

$$(\nabla^2 + k^2)A(\boldsymbol{r}) = 0. \tag{5}$$

This choice assures the correct symmetry of linearly polarized modes. $\boldsymbol{A}_{\mathrm{e}}, \boldsymbol{A}_{\mathrm{m}}$ are related to the electric and magnetic fields by

$$\boldsymbol{E} = (\mathrm{i}\omega/2)[\boldsymbol{A}_{\mathrm{e}} + \frac{1}{k^2}\nabla(\nabla\cdot\boldsymbol{A}_{\mathrm{e}}) + \frac{1}{k}\nabla\times\boldsymbol{A}_{\mathrm{m}}], \tag{6}$$

$$Z_{\mu\varepsilon}\,\boldsymbol{H} = (\mathrm{i}\omega/2)[\boldsymbol{A}_{\mathrm{m}} + \frac{1}{k^2}\nabla(\nabla\cdot\boldsymbol{A}_{\mathrm{m}}) + \frac{1}{k}\nabla\times\boldsymbol{A}_{\mathrm{e}}], \tag{7}$$

which can be proved by inserting these expressions in Maxwell's curl equations above and making use of Eq. (5). Thus, the problem is reduced to solving the scalar Helmholtz equation, Eq. (5).

Since we are interested in beams propagating along the z-axis, we make the following ansatz for the scalar field A:

$$A(\tilde{x}, \tilde{y}, \tilde{z}) = A_0\,\psi(\tilde{x}, \tilde{y}, \tilde{z})\,\mathrm{e}^{\mathrm{i}\tilde{z}/s^2}. \tag{8}$$

A_0 denotes a constant amplitude ψ and is a dimensionless function. In Eq. (8) we used the normalized coordinates

$$\tilde{x} = x/w_0, \qquad \tilde{y} = y/w_0, \qquad \tilde{z} = z/(kw_0^2), \tag{9}$$

where w_0 denotes the beam waist radius of the fundamental Gaussian beam and

$$s = \frac{1}{kw_0} = \frac{1}{\sqrt{\mu\varepsilon}}\frac{\lambda}{2\pi w_0}. \tag{10}$$

Introducing the transverse Laplace operator $\tilde{\nabla}_{\mathrm{t}}$ which acts on the normalized coordinates $(\tilde{x}, \tilde{y})$, Eq. (5) leads to a differential equation for the function ψ:

$$\left[\tilde{\nabla}_{\mathrm{t}} + 2\mathrm{i}\frac{\partial}{\partial\tilde{z}}\right]\psi(\tilde{x}, \tilde{y}, \tilde{z}) = -s^2\frac{\partial^2}{\partial\tilde{z}^2}\psi(\tilde{x}, \tilde{y}, \tilde{z}). \tag{11}$$

In order to solve this equation we introduce for ψ a series expansion in even powers of the parameter s:

$$\psi = \psi_0 + s^2\psi_2 + s^4\psi_4 + \ldots\,. \tag{12}$$

It is apparent that the larger the parameter s is (tight focus), the slower the convergence will be. Inserting the series expansion in Eq. (11) leads to

$$\left[\tilde{\nabla}_{\mathrm{t}} + 2\mathrm{i}\frac{\partial}{\partial\tilde{z}}\right]\psi_0 = 0, \tag{13}$$

$$\left[\tilde{\nabla}_{\mathrm{t}} + 2\mathrm{i}\frac{\partial}{\partial\tilde{z}}\right]\psi_{(2n+2)} = -\frac{\partial^2}{\partial\tilde{z}^2}\psi_{2n}, \quad n = 0,1,2,\ldots\,. \tag{14}$$

The first equation is the familiar paraxial beam equation. It leads to purely transverse solutions [17] denoted as TEM. In order to account for longitudinal field components, higher terms in the series expansion have to be considered. Once an accurate solution for ψ is determined, the electric and magnetic fields can be derived from Eqs. (6)–(8).

The fundamental Gaussian beam solution of Eq. (13) has the well-known form

$$\psi_0(\tilde{x}, \tilde{y}, \tilde{z}) = \sigma e^{-\sigma\tilde{\rho}^2} \quad \text{with } \sigma(\tilde{z}) = (1 + 2i\tilde{z})^{-1}, \quad (15)$$

where $\tilde{\rho}$ denotes the normalized radial distance $(\tilde{x}^2 + \tilde{y}^2)^{1/2}$. Higher-order correction terms $\psi_{(2n+2)}$ can be determined by solving Eq. (14). Expressions for ψ_2 and ψ_4 are provided by Barton and Alexander [19]. Using the expressions for ψ_0, ψ_2 and ψ_4 one obtains fifth-order corrected expressions for the electric and magnetic fields of the fundamental Gaussian beam. These fields are shown in Fig. 2 for $s = 0.25$. The longitudinal electric field

$$E_z = -iE_0\tilde{x}[s(2\sigma) + s^3(6\tilde{\rho}^2\sigma^3 - 2\tilde{\rho}^4\sigma^4) + s^5(20\tilde{\rho}^4\sigma^5 - 10\tilde{\rho}^6\sigma^6 + \tilde{\rho}^8\sigma^7) + \ldots]\psi_0 e^{i\tilde{z}/s^2} \quad (16)$$

is due to higher-order correction terms and is larger for tighter foci (large parameter s). For large distances $\tilde{z}$, powers of σ higher than one can be neglected and the TEM approximation of the Gaussian beam is retained. In this case, the beam shape becomes a hyperboloid whose asymptotes enclose an angle

$$\theta = 2/kw_0 = 2s \quad (17)$$

with the z-axis. The parameter s is therefore a direct measure for the convergence of a beam and hence the numerical aperture of a corresponding focusing lens. The tighter the focus of the beam is the more higher-order correction terms have to be included. The accuracy of the series expansion in the vicinity of the focus has been discussed in Ref. [19]. However, for very tight foci ($s \to 1$) the convergence is so poor that the series expansion fails. In this case the fields have to be represented by an angular spectrum involving numerical integrations.

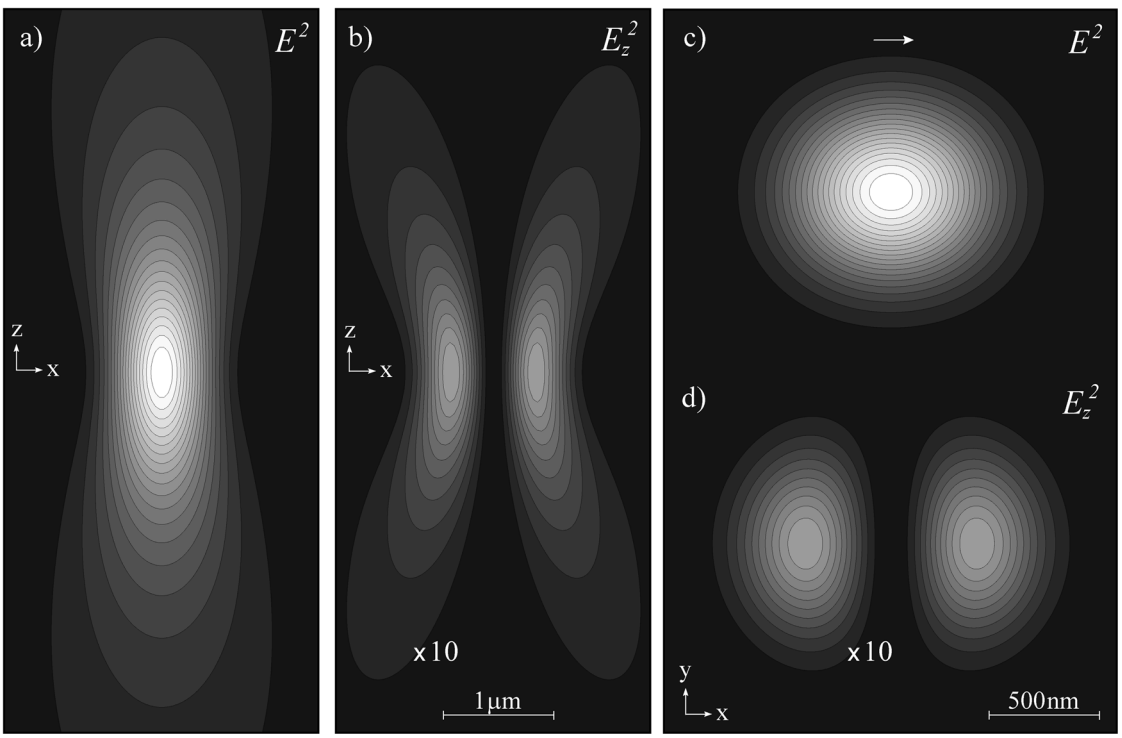

Fig. 2. Focal region of the fundamental Gaussian beam ($s = 0.25$, $\lambda = 800$ nm). The beam propagates along the z axis. The figures show the electric energy density of the total field [(a) and (c)] and the longitudinal field [(b) and (d)]. The polarization is indicated by the arrow in figure (c). Linear scaling with increments of $0.05E_0^2$ in (a) and (c) and increments of $0.005E_0^2$ in (b) and (d) starting from a level of 0.

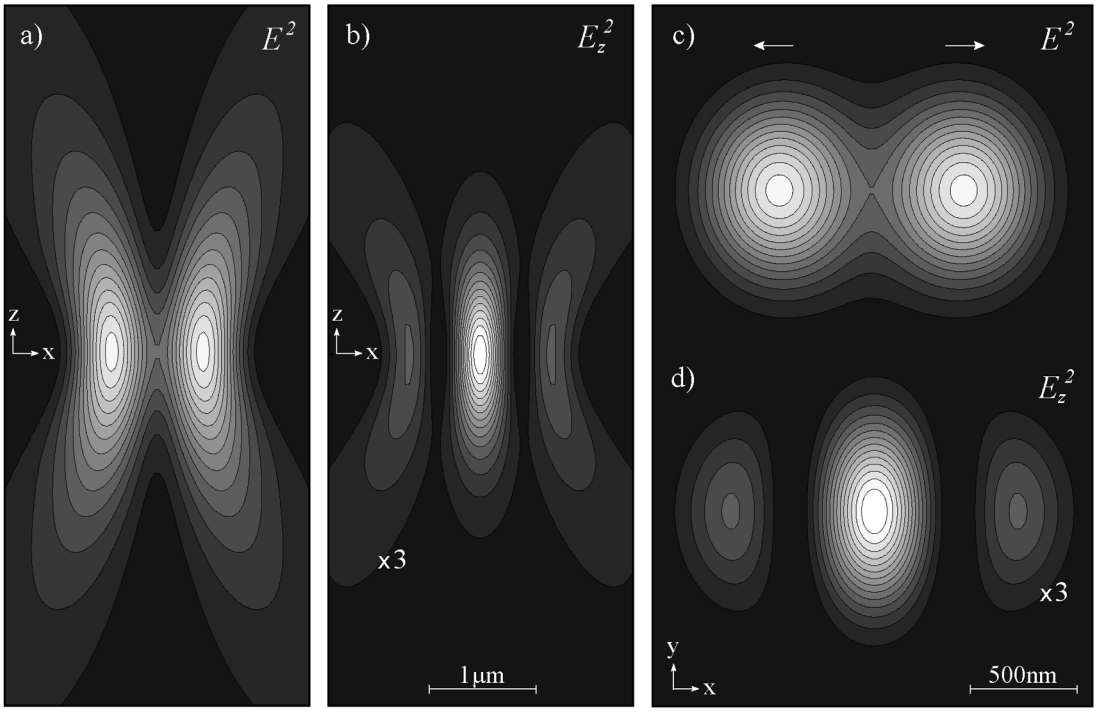

Fig. 3. Focal region of the Hermite–Gaussian (1,0) beam ($s = 0.25$, $\lambda = 800$ nm). The beam propagates along the z axis. The figures show the electric energy density of the total field [(a) and (c)] and the longitudinal field [(b) and (d)]. The polarization is indicated by the arrows in figure (c). The two halfs of the beam are 180° out of phase. Linear scaling with increments of $0.05E_0^2$ in (a) and (c) and increments of $0.0166E_0^2$ in (b) and (d) starting from a level of 0.

The fields of the fundamental mode can be used to derive higher-order modes. Since the fundamental Gaussian mode is a solution of a linear homogeneous partial differential equation (Helmholtz equation), any combination of spatial derivatives of the fundamental mode is also a solution to the differential equation. As Zauderer [20] pointed out, Hermite–Gaussian modes $\boldsymbol{E}^{\mathrm{H}}_{n,m}$ can be generated from the fundamental mode $\boldsymbol{E}$ according to

$$\boldsymbol{E}^{\mathrm{H}}_{n,m}(\tilde{x},\tilde{y},\tilde{z}) = \frac{\partial^n}{\partial\tilde{x}^n}\frac{\partial^m}{\partial\tilde{y}^m}\boldsymbol{E}(\tilde{x},\tilde{y},\tilde{z}). \tag{18}$$

Once an accurate solution for the fundamental Gaussian mode (Eq. (16)) is obtained, any higher-order mode can be generated by simply applying Eq. (18). Fig. 3 shows the fields of the Hermite–Gaussian (1,0) mode which has a non-vanishing longitudinal field along its propagation axis

$$\begin{aligned} E^{\mathrm{H}}_{1,0_z} = \mathrm{i}E_0[&s(4\tilde{x}^2\sigma^2 - 2\sigma) + s^3(2\tilde{\rho}^4\sigma^4 - 6\tilde{\rho}^2\sigma^3 \\ &+ 20\tilde{x}^2\tilde{\rho}^2\sigma^4 - 12\tilde{x}^2\sigma^3 - 4\tilde{x}^2\tilde{\rho}^4\sigma^5) \\ &+ s^5(10\tilde{\rho}^6\sigma^6 - 20\tilde{\rho}^4\sigma^5 - \tilde{\rho}^8\sigma^7 \\ &+ \tilde{x}^2\{-28\tilde{\rho}^6\sigma^7 + 100\tilde{\rho}^4\sigma^6 - 80\tilde{\rho}^2\sigma^5 \\ &+ 2\tilde{\rho}^8\sigma^8\}) + \ldots]\psi_0 \mathrm{e}^{\mathrm{i}\tilde{z}/s^2}. \end{aligned} \tag{19}$$

As indicated by the arrows in Fig. 3c, the polarizations of the individual maxima are 180° out of phase. On the z axis, the longitudinal field is entirely determined by the first-order correction term and is 90° out of phase with respect to the transverse field. For very tight foci, it can be shown that the longitudinal field amplitude can be almost as large as the transverse field amplitude. To the first order, the ratio of the two is linear in s. It has to be emphasized, that other Hermite–Gaussian modes,

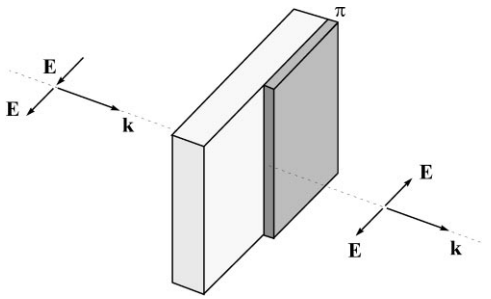

Fig. 4. Generation of a Hermite–Gaussian (1,0) beam. A fundamental Gaussian beam is bisected at the edge of a 180° phase plate. The polarization of the incident beam is perpendicular to the edge of the phase plate. The arrangement delays one half of the beam by 180° and therefore favours the conversion to the Hermite–Gaussian (1,0) mode.

such as (0,1) and (1,1) modes, do not necessarily provide a longitudinal field on the beam axis. Notice that doughnut shaped modes are superpositions of Hermite–Gaussian modes. It can also be shown that Laguerre–Gaussian modes can be expressed by a finite superposition of Hermite–Gaussian modes [20].

Although laser beams can be adjusted to a higher mode by manipulating the laser resonator, it is desirable to convert a fundamental Gaussian beam into a higher-order mode *externally* without perturbing the laser characteristics. However, such a conversion cannot be realized by linear operations, such as interferences, on separated laser beams. This becomes obvious when considering a certain laser mode as a mathematical eigenfunction. The linear superposition of given eigenfunctions cannot generate a new, linearly independent eigenfunction. However, the conversion between modes can be realized by inserting phase plates into different regions in the beam cross-section [21]. As shown in Fig. 4, the conversion to the Hermite–Gaussian (1,0) mode is favoured by bisecting the fundamental Gaussian beam by the edge of a thin phase plate which shifts the phase of one half of the beam by 180°. The incident beam has to be polarized perpendicular to the edge of the phase plate. A different approach to create higher-order modes is based on an external four-mirror ring cavity as recently described in Ref. [22].

2.2. Laser beams incident along the axis of a metal tip

In Fig. 5 the fifth-order corrected fields for the (0,0) and (1,0) modes are used to illuminate a sharply pointed gold tip (5 nm tip radius) along the tip axis. The two beams are focused on the foremost part of the tip and have a focal parameter of $s = 0.25$. This corresponds to a beam waist radius of $w_0 = 1/(sk) = 0.64\lambda$ and a convergence angle of $\theta = 28.65°$. The wavelength of the incident beams is adjusted for two-photon fluorescence measurements (Ti : sapphire $\lambda = 800$ nm) to lower the background signal. To solve the three-dimensional Maxwell's equations for the configuration of Fig. 5, the multiple multipole method [23] has been applied. The figures show the electric field (E^2) in the plane of polarization [(x,z) plane of Figs. 2 and 3]. As expected, no field enhancement is observed if the tip is illuminated with the Gaussian beam. It can be observed, that even a shadow exists in front of the tip. Because of a moderate enhancement at the sides of the tip, the field extends over a large area. Illumination with the Hermite–Gaussian (1,0) mode, on the other hand, leads to an intensity enhancement of ≈ 1000. This number can be significantly increased by using sharper tips, smaller taper angles, a tighter focus (larger parameter s) and longer wavelengths. The field consists mainly of evanescent components which decay rapidly with distance from the tip. With decreasing tip radius, the lateral confinement becomes stronger and the field decays faster. Close to the tip, the field resembles the field of a vertical dipole located inside the tip. As shown in Fig. 5 the fields partially penetrate into the tip. The dissipated energy heats the tip and gives rise to a temperature increase. However, as shown in Ref. [7] this increase is negligible for laser intensities below $\approx 100\,\mathrm{mW/\mu m^2}$.

The field enhancement effect is associated with a strong induced surface charge density (Fig. 6). The incident light drives the free electrons in the metal along the direction of polarization. While the charge density is zero inside the metal at any instant of time ($\nabla \cdot \boldsymbol{E} = 0$), charges accumulate on the surface of the metal. When the incident polarization is perpendicular to the tip axis (Fig. 5a), diametrically opposed points on the tip surface have

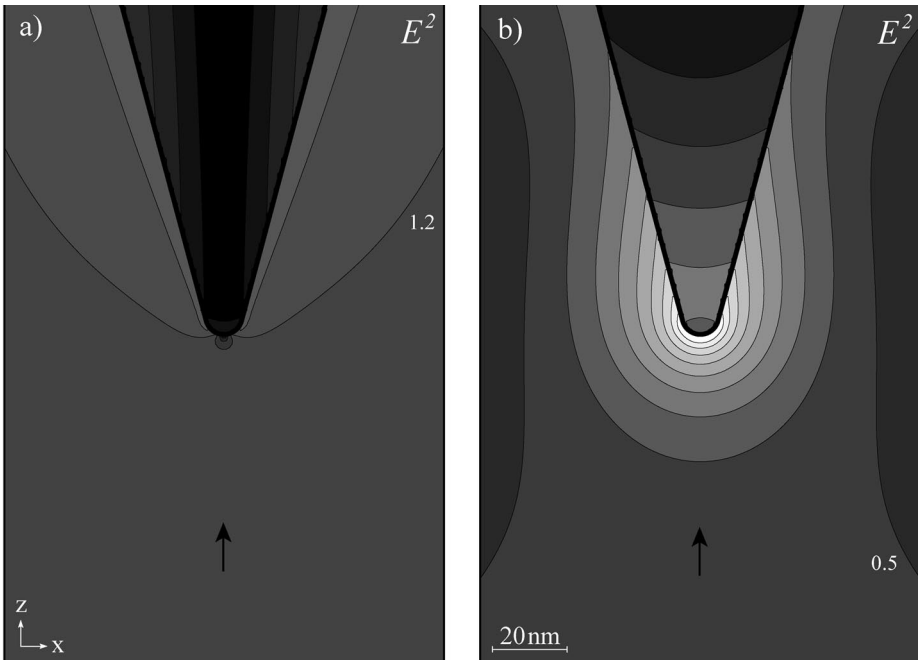

Fig. 5. Field enhancement at a gold tip. The tip is in the focus of (a) a fundamental Gaussian beam and (b) a Hermite–Gaussian (1,0) beam. The beam has a focal parameter of $s = 0.25$ and is incident along the axis of the tip. The strong enhancement in (b) is induced by the longitudinal field component of the (1,0) mode. Both figures show E^2 on a logarithmic scale (factor of 2 between successive lines). The scaling is given by the numbers in the figures (multiples of the exciting field). The dielectric constant of gold at $\lambda = 800$ nm is $\varepsilon = -24.1 + i1.5$ and the tip radius is 5 nm.

opposite charges. As a consequence, the foremost end of the tip remains uncharged. On the other hand, when the incident polarization is parallel to the tip axis (Fig. 5b), the induced surface charge density is rotationally symmetric and has the highest amplitude at the end of the tip. The surface charges form an oscillating, standing wave with a wavelength smaller than the wavelength of the illuminating light. The charge waves have therefore the characteristics of surface plasmons. We note, however, that in the present case the excitation is far from plasmon resonance. It is important to emphasize that for dielectric materials, such as quartz and silicon, no field enhancement is present.

If the enhanced field of the tip is used to image single molecules deposited on the surface of a planar substrate, the resulting fluorescence images will be proportional to $|\boldsymbol{p}\cdot\boldsymbol{E}|^2$, where $\boldsymbol{p}$ is the transition dipole moment of the molecule. Thus, the molecular fluorescence can be used to probe the exciting field [24]. Assuming the molecular fluorescence is not entirely quenched by the tip, Fig. 7 shows calculated fluorescence scan-images for sample molecules with different dipole orientations. The orientations of the dipoles relative to the sample surface are indicated in the figures. Since the exciting field close to the tip is almost rotationally symmetric (vertical dipole), molecules with parallel transition dipoles show always double-spotted patterns. The molecular dipole axis corresponds to the vector pointing from one spot to the other. A molecule with a vertical dipole shows only one spot. It is therefore possible to map the spatial orientation of the molecular dipole moments with high accuracy. Furthermore, for horizontal dipoles, the spacing between the two spots is a direct measure of the tip diameter.

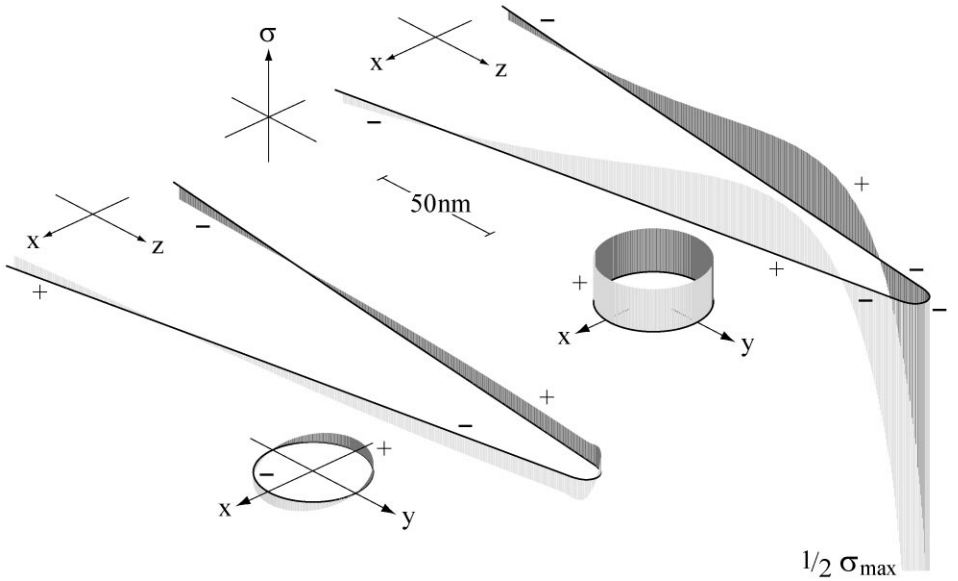

Fig. 6. Induced surface charge density (σ) corresponding to a situation similar to Fig. 5a (left) and Fig. 5b (right), respectively. The surface charges form a standing wave in each case. In Fig. 5a, the surface charge wave has a node at the end of the tip, whereas in Fig. 5b there is a large surface charge accumulation at the foremost part, responsible for the field enhancement. From Ref. [7].

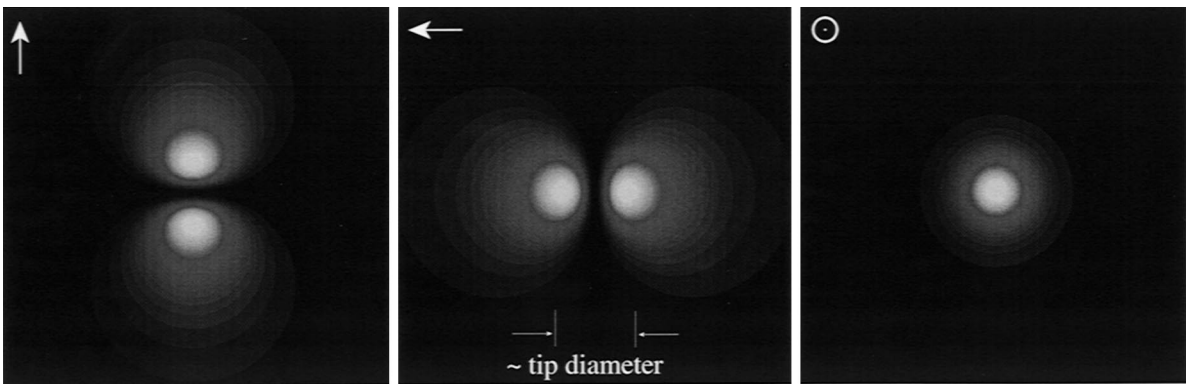

Fig. 7. Simulation of fluorescence images of single molecules. The molecules are located on a transverse plane below the tip shown in Fig. 5b. The orientations of the transition dipoles are indicated by the arrows. A tip sample separation of 2 nm is assumed. The patterns of the horizontal dipoles are amplified by a factor of 5.

3. Conclusions

We introduced a new scheme for high-resolution optical imaging. The scheme relies on the field enhancement at sharply pointed metal tips. In order to keep the exposure area small, the tip is illuminated along the tip axis with a tightly focused Hermite–Gaussian (1,0) laser beam mode. In the focal region, this mode has a longitudinal field component which is needed for establishing the field enhancement. The Hermite–Gaussian (1,0) mode can be generated by a $\lambda/2$ phase plate which delays one half of an incident Gaussian beam. To ensure sufficient background discrimination,

nonlinear responses of the sample, such as two-photon fluorescence or generation of second/third harmonics, are detected. This requires the use of high repetition-rate femtosecond lasers. The resolution of the proposed scheme is expected to be on the order of the tip diameter.

Acknowledgements

This research was supported by the US Department of Energy's (DOE) Energy Research Laboratory Technology Application program. Pacific Northwest National Laboratory is operated for DOE by Battelle Memorial Institute under contract DE-AC06-76RLO 1830.

References

[1] E. Betzig, J.K. Trautman, Science 257 (1992) 189.
[2] F. Zenhausern, M.P. O'Boyle, H.K. Wickramasinghe, Appl. Phys. Lett. 65 (1994) 1623.
[3] For a review, see X.S. Xie, Acc. Chem. Res. 29 (1996) 598.
[4] J.J. Macklin, J.K. Trautman, T.D. Harris, L.E. Brus, Science 272 (1996) 255.
[5] H.P. Lu, X.S. Xie, Nature 385 (1997) 143.
[6] R.C. Dunn, G.R. Holtom, L. Mets, X.S. Xie, J. Phys. Chem. 98 (1994) 3094.
[7] L. Novotny, R.X. Bian, X.S. Xie, Phys. Rev. Lett. 79 (1997) 645.
[8] O.J.F. Martin, C. Girard, Appl. Phys. Lett. 70 (1997) 705.
[9] L. Novotny, D.W. Pohl, B. Hecht, Opt. Lett. 20 (1995) 970.
[10] W. Denk, D.W. Pohl, J. Vac. Sci. Technol. B 9 (1991) 510.
[11] A. Lahrech, R. Bachelot, P. Gleyzes, A.C. Boccara, Opt. Lett. 21 (1996) 1315.
[12] S. Kawata, Y. Inouye, Ultramicroscopy 57 (1995) 313.
[13] A.A. Gorbunov, W. Pompe, Phys. Stat. Sol. A 145 (1994) 333.
[14] J. Jersch, K. Dickmann, Appl. Phys. Lett. 68 (1996) 868.
[15] E.J. Bochove, G.T. Moore, M.O. Scully, Phys. Rev. A 46 (1992) 6640, and references therein
[16] J.K. Trautman, presentation at the biophysical meeting in Baltimore, Maryland, 1996.
[17] A. Yariv, Quantum Electronics, 3rd ed., Wiley, New York, 1989.
[18] H.S. Green, E. Wolf, Proc. Phys. Soc. A 66 (1953) 1129.
[19] J.P. Barton, D.R. Alexander, J. Appl. Phys. 66 (1989) 2800.
[20] E. Zauderer, J. Opt. Soc. Am. A 3 (1986) 465.
[21] C. Haupt, E. Jäger, A. Rothe, M. Daffner, H.J. Tiziani, Proc. SPIE 1983, 658 (1993).
[22] M.J. Snadden, A.S. Bell, R.B.M. Clarke, E. Riis, D.H. McIntyre, J. Opt. Soc. Am. A 14 (1997) 544.
[23] C. Hafner, The Generalized Multiple Multipole Technique for Computational Electromagnetics, Artech, Boston, 1990.
[24] E. Betzig, R.J. Chichester, Science 262 (1993) 1422.